Micromachined High-Aspect-Ratio Parylene Spring and Its Application to Low-Frequency Accelerometers

Yuji Suzuki, *Member, IEEE, ASME, Member*, and Yu-Chong Tai, *Fellow, IEEE*

***Abstract*—A new microfabrication technology for high-aspect-ratio parylene structure has been developed for soft spring applications. Free-standing parylene beams with widths of 10–40 μm and aspect ratios of 10–20 have been successfully fabricated. Since parylene has a small Young's modulus, a high-aspect-ratio beam with a spring constant of the order of 1×10^{-3} N/m has been realized. The large yield strain of parylene enables a test structure to have a large-amplitude oscillation of 600 $\mu m_{p\text{-}p}$, without any failure of the high-aspect-ratio springs. An early prototype of in-plane capacitive accelerometer was also developed. It was found that its resonant frequency is as low as 37 Hz, and the noise spectral density is 64 $\mu g/(Hz)^{0.5}$. [1606]**

***Index Terms*—Capacitive accelerometer, high-aspect-ratio beam, low spring constant, parylene.**

I. Introduction

FOR mechanical transducers with a high sensitivity, a soft beam with a low spring constant is required. However, since conventional MEMS materials such as single crystal Si have a large Young's modulus, it is not a straightforward process to develop soft structures. Weigold *et al.* [1] developed a Si accelerometer with a low spring constant of 0.127 N/m. However, very thin beams of 1 μm in width and 450 μm in length were required. An alternative approach for producing a soft spring is to use photosensitive polymer materials [2]–[4]. Lee *et al.* [4] employed SU-8 to make a cantilever beam for atomic force microscopy with a spring constant of 0.248 N/m. However, SU-8 is not suitable for mechanical structures requiring high accuracy due to its large internal stress and a relatively large thermal coefficient of expansion (TCE) of 5×10^{-5}/K.

Parylene (poly-para-xylylene) is known as a MEMS- compatible polymer that can be deposited with a CVD process, and is now attracting increasing attention for possible use in mechanical and fluidic micro devices [5]–[12]. Its physical properties and detailed internal stress characteristics have previously been reported [13], [14]. The advantage of using parylene for mechanical parts is threefold. Firsty, parylene has a small Young's modulus ($\sim$ 4 GPa), which makes it easy to design soft springs with. Second, parylene is a nonbrittle material with a large linear-elastic range (yield strain $\sim 3\%$), which allows a large deflection without failure. Third, parylene has a 30% lower TCE than SU-8 or polyimide.

The final goal of the present study is to develop micro-fabrication technology to be used to produce soft springs for in-plane transducers such as accelerometers [15]–[20] and energy harvesting devices [21], [22]. For these devices, sensitivity to mechanical force should vary by orders of magnitude depending on the direction. The structure should be soft in the direction of interest, but at the same time, it should be rigid in the other two perpendicular directions to minimize mechanical cross-talk. Therefore, high-aspect-ratio structures (HARS) are required.

The most straightforward approach to achieve HARS is to use deep-reactive ion etching (DRIE) of a Si substrate, such as the Bosch process [23]. HEXSIL [24], [25] and HARPSS [26] have also been proposed for high-aspect structures, where deep trenches are refilled with poly-Si. However, both single crystal Si and poly-Si are brittle, so mechanical failure is of considerable concern. Alternatively, high-aspect-ratio metal structures can be fabricated by the LIGA [27] process, but it requires X-ray, which is generally a much more expensive process. Moreover, all the existing technologies use materials with a large Young's modulus, which is larger than 100 GPa.

The objectives of the present study are to develop a new microfabrication technology for high-aspect-ratio parylene beams with a small spring constant, and to characterize their mechanical performance. We also present the first in-plane accelerometer using the parylene high-aspect-ratio beams.

II. Fabrication of Parylene High-Aspect-Ratio Structures

The main process flow for the high-aspect-ratio parylene beam fabrication is shown in Fig. 1. The process starts with 4" Si wafers with 2-μm-thick thermal oxide. The upper SiO_2 is patterned with buffered HF [see Fig. 1(a)] for the etch mask of DRIE, and 300–400-μm-deep trenches are etched into the substrate [see Fig. 1(b)]. The trenches are used as parylene molds and their depth defines the desired height of the beams. After stripping away the remaining SiO_2, a second 2-μm-thick thermal oxide is grown on all exposed Si surfaces as the etch-stop layer for the later DRIE [see Fig. 1(c)]. This is followed by a parylene-C deposition with a thickness of 10–20 μm to refill the trenches [see Fig. 1(d)]. The deposition pressure is chosen as 22 mT. The parylene film is then etched

Manuscript received May 18, 2005; revised January 20, 2006. This work was supported by the NSF Engineering Research Center (ERC), California Institute of Technology, Pasadena. The work of Y. Suzuki was supported by Professor N. Kasagi of the University of Tokyo. Subject Editor R. R. A. Syms.

Y. Suzuki is with the Department of Mechanical Engineering, University of Tokyo, Tokyo 113-8656, Japan (e-mail: ysuzuki@thtlab.t.u-tokyo.ac.jp).

Y.-C. Tai is with the Department of Electrical Engineering, California Institute of Technology, Pasadena, CA 91125 USA.

Digital Object Identifier 10.1109/JMEMS.2006.879706

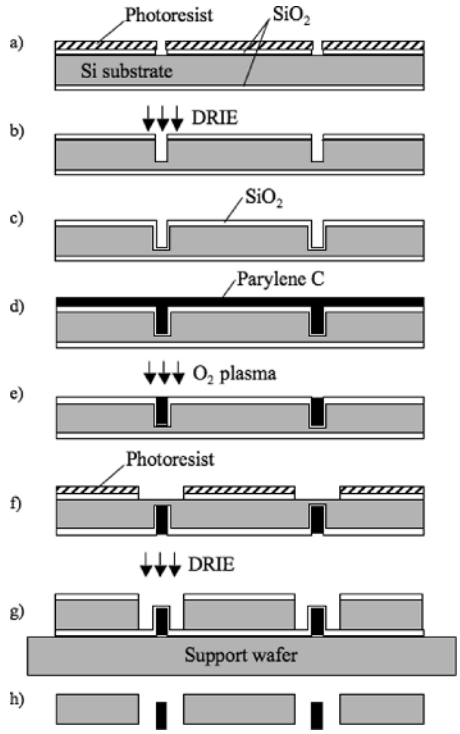

Fig. 1. Process flow for the high-aspect-ratio parylene structure. (a) Wet oxidation and patterning SiO_2. (b) Etch trench by DRIE. (c) Stripping SiO_2 and making the second wet oxidation. (d) Deposit of 20 μm-thick parylene-C. (e) Etch-back parylene with O_2 plasma. (f) Pattern SiO_2 on the backside of the wafer. (g) Gluing onto a support wafer and etching through using DRIE. (h) Stripping SiO_2 and the release of parylene structures with buffered HF.

back using O_2 plasma [Fig. 1(e)]. Next, the wafer is flipped over and etch windows are patterned into the backside SiO_2 with buffered HF [see Fig. 1(f)]. After dicing the wafer into individual die, each die is glued onto a support wafer, and the silicon is etched away from the backside with DRIE to expose the parylene beams, which are covered by the etch-stop SiO_2 [see Fig. 1(g)]. Finally, the beams are completely freed by stripping the SiO_2 away with buffered HF [see Fig. 1(h)].

Fig. 2(a) shows an SEM image of a 20-μm-wide trench as deposited. Clearly, the parylene-C deposition is conformal, and the film thickness is almost uniform even inside the deep trench. This is because the mean free path of parylene molecules is as small as a few cm, and also because the sticking coefficient, which is defined by the ratio between the number of molecules reacting with a radical chain end and the number of incident monomer molecules onto the surface, is as low as 1×10^{-4} at room temperature [28].

Also visible is a small void inside, which is often observed in parylene deposition onto trenches [29]. The void is caused because the top part of the trench is sealed at an early stage of the deposition. The timing when the top part of the trench is sealed with parylene depends on the trench width, and the time duration before the trench is sealed multiplied by the deposition rate determines the film thickness inside the trench. For 40-μm -wide trenches, the film thickness inside is about 17 μm. The film thickness inside the trench decreases with the trench width, and becomes 10, 7, and 2.5 μm, respectively, for 30-, 20-, and 10-μm-wide trenches.

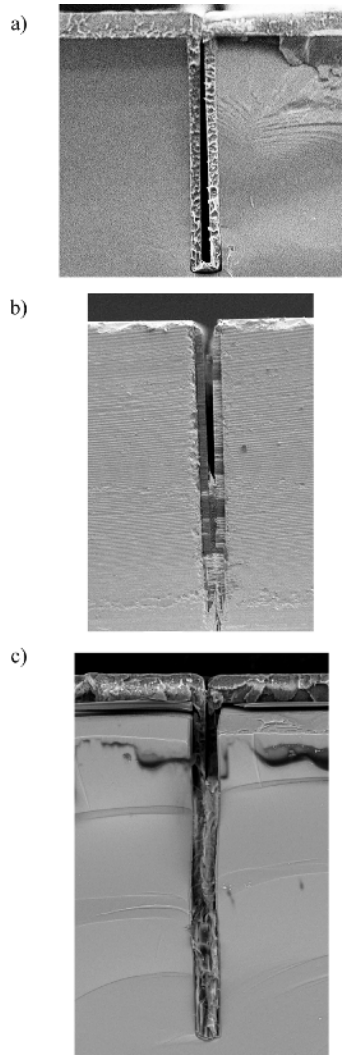

Fig. 2. Cross-sectional SEM images of a 20-μm-wide trench. (a) As deposited. (b) After the etchback. (c) After the second deposition of 20-μm-thick parylene-C.

After etch-back of the parylene film with O_2 plasma, the top part of the trench is opened [see Fig. 2(b)]. If desirable, this void can be completely eliminated with a second parylene-C deposition [see Fig. 2(c)]. The maximum aspect ratio fabricated here was 20, but trenches with higher aspect ratios can also be filled with parylene, once the trench itself is etched with DRIE.

Fig. 3(a) shows an SEM image of a free-standing cantilever beam 30 μm in width, 400 μm in height, and 2.5 mm in length (aspect ratio of 13.3). A triangle-shaped trench etched into the substrate works well as an anchor. Fig. 3(b) shows a leaf spring structure with an aspect ratio of 17.5. Si islands surrounded by parylene beam are successfully etched out with DRIE, and only free-standing complex parylene structures remain.

Fig. 4 shows parylene high-aspect-ratio beams of 10–40 μm in width. The 30- and 40-μm-wide beams are 400–μm high, and the 10- and 20-μm-wide beam structures are, respectively, about 200 μm and 350 μm in height due to the RIE lag. Parylene film is known to be in compressive stress as it is deposited, but that becomes tensile stress after thermal annealing [13], [14]. In the present study, the parylene film undergoes baking at 100–110

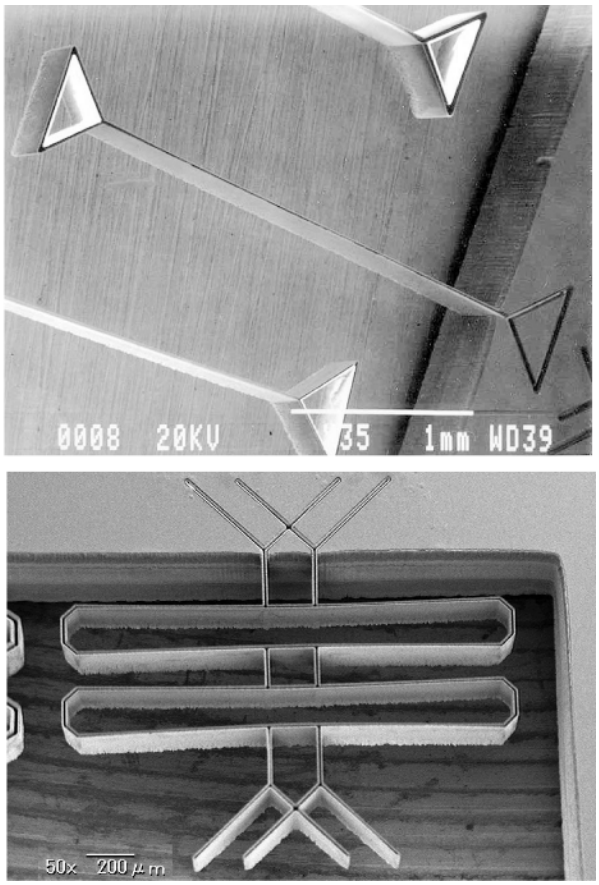

Fig. 3. SEM images of high-aspect-ratio free-standing parylene structures. (a) Cantilever beam 30 μm in width, 400 μm in height and 2.5 mm in length. (b) Leaf spring structure using a parylene beam 20 μm in width and 350 μm in height.

°C for the lithography step of the etch windows on the backside [see Fig. 1(f)], and the beams are actually in tensile stress when released.

It is now clear that complex high-aspect-ratio parylene structures with aspect ratios up to 20 can be successfully fabricated through the present MEMS process. Static and dynamic characteristics of the structures are discussed in the next chapter.

III. Evaluation of Parylene High-Aspect-Ratio Beam

Fig. 5 shows a magnified view of a pendulum structure with a 10-μm-wide beam, of which the aspect ratio is 20. The Si mass dimensions are 700 μm× 700 μm× 530 μm. The device was fixed onto a gonio stage, and the force in the in-plane direction is changed by altering the tilt angle. Fig. 6 shows the deflection of the cantilever beam versus the force in the in-plane direction. It was discovered that the spring constant is as low as 0.0045 N/m. The spring constant obtained is three times smaller than the value estimated with conventional beam theory. This is probably because the trench is not fully filled with parylene as shown in Fig. 2(b), and the cross section of the beams is U-shaped. On the other hand, this soft spring is robust and will not fracture even by shaking vigorously.

The spring constant for thicker beams was estimated from measurements of their resonant frequency. The measured values are, respectively, 0.0261, 0.169, and 0.484 N/m for 20-, 30-, and

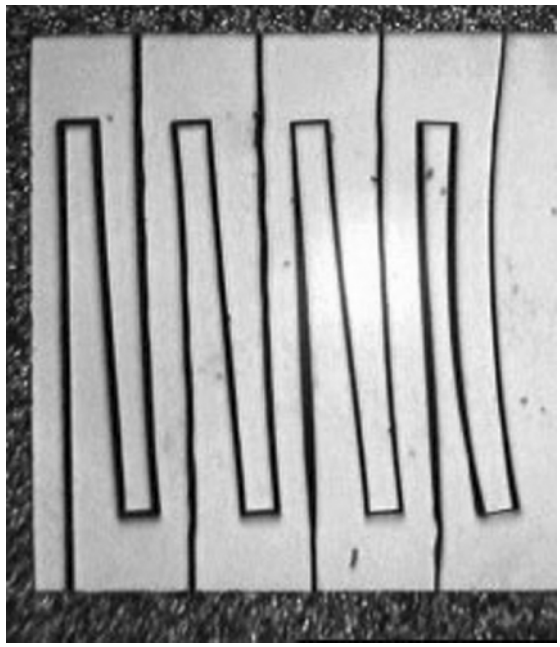

Fig. 4. Beam structures under tensile stress. Left to right, 40-, 30-, 20-, and 10-μm-wide beam structures.

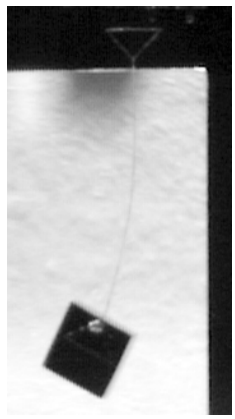

Fig. 5. A pendulum structure with a 10-μm-wide beam suspending 700 μm× 700 μm Si substrate under a gravity force.

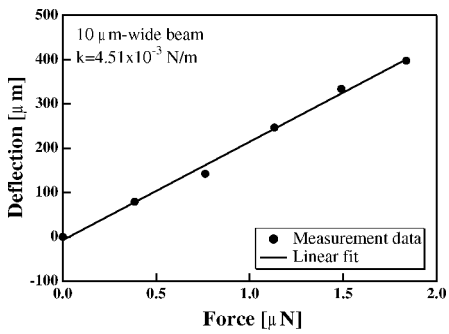

Fig. 6. Spring constant measurement of a 10-μm-wide beam.

40-μm-wide beams. Again, the measurement results are 3–7 times smaller than the designed values using the beam theory.

In order to study the dynamic response of parylene beams, test structures with a 1.75 mm × 1.75 mm Si proof mass, supported by two parylene leaf springs [see Fig. 7(a)], were fab-

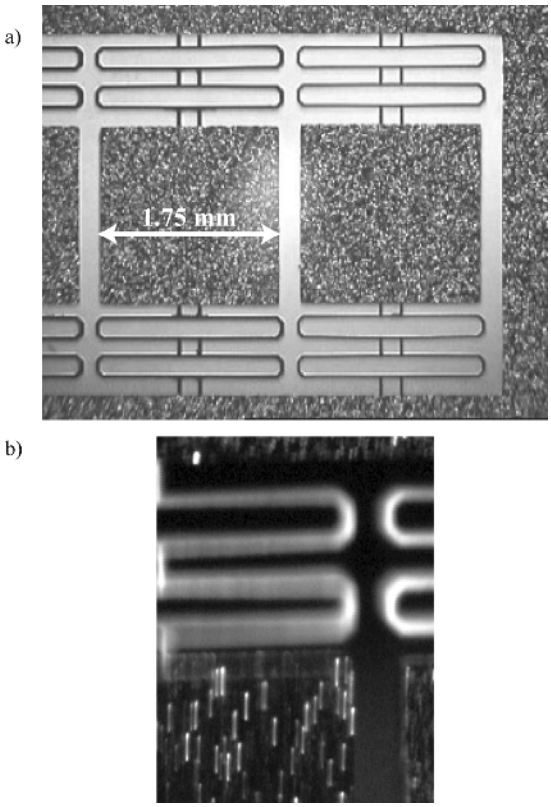

Fig. 7. Test structures with two high-aspect-ratio leaf springs and a 1.75 mm × 1.75 mm mass in between, as seen from the unpolished side. (a) Left to right: 40-, 30-, and 20-μm-wide leaf springs. (b) Magnified view of the proof mass in oscillation.

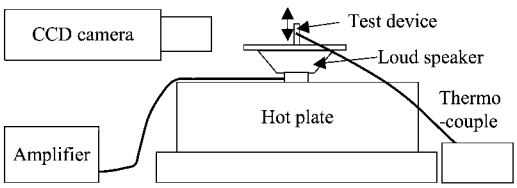

Fig. 8. Schematic of the experimental setup for the dynamic response measurement.

ricated. Fig. 8 shows the experimental setup. The device was glued onto a loud speaker and shaken in the in-plane direction at prescribed frequencies and amplitudes. Relative displacement of the proof mass to the substrate was measured visually using a CCD camera equipped with a high-magnification lens. Since the framing speed of the CCD camera is much slower than the oscillation frequency, the amplitude of the proof mass is measured from the streak length of the surface pattern as shown in Fig. 7(b). The resolution of the present amplitude measurement is one pixel of the image, which corresponds to about 3 μm.

Fig. 9 shows the dynamic response of a proof mass with 20-μm-wide springs. The measurement data fit well with a simple spring-mass-damper model. The resonant frequency $f_{\rm res}$ and the quality factor Q are determined by a curve fit, and they are 112.9 and 15.1 Hz, respectively. The peak-to-peak amplitude at the resonance is as large as 600 μm. The spring constant of each leaf spring structure is 0.9 N/m. The resonant

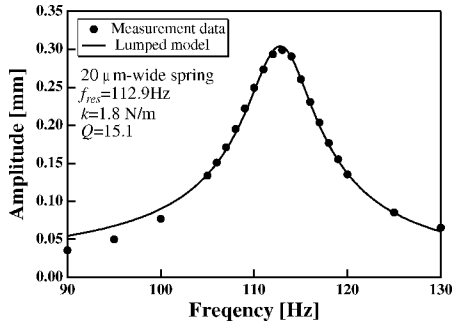

Fig. 9. Frequency response of the test structure with 20-μm-wide high-aspect-ratio leaf springs.

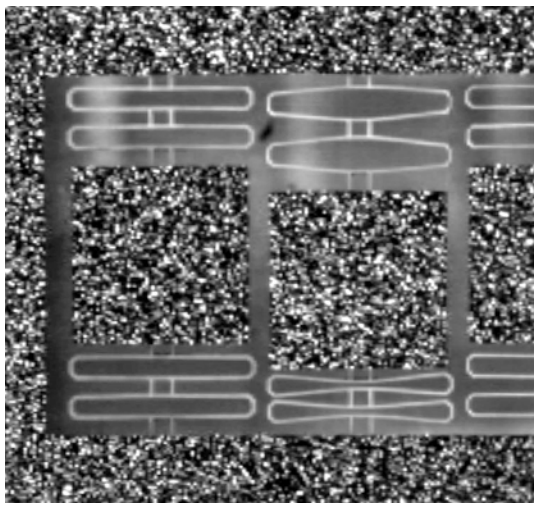

Fig. 10. A snap shot of the test structure with 30-μm-wide high-aspect-ratio leaf springs at the resonant frequency ($\sim$ 257 Hz). Left to right: 40-, 30-, and 20-μm-wide leaf springs.

frequencies for 30-, and 40-μm-wide beams are, respectively, 257 and 410 Hz.

Fig. 10 shows a snap-shot of the test structures at the oscillation frequency of 257 Hz. Only the structure with 30 μm-wide springs is resonating. Because of the large oscillation amplitude, beams on the shrunk side are almost attached to each other. However, the springs undergo neither any damage nor plastic deformation. It is noted that the resonant frequency of these leaf springs remains unchanged even after being driven at their resonant frequency oscillation for several hours, which corresponds to about 2×10^6 cycles. These findings confirm the robustness of parylene beams because of its large yield strain.

The effect of temperature on the spring constant of the high-aspect-ratio parylene springs was also examined. The device temperature was measured with a thermocouple, and ramped at about 1 °C/min. with a hot plate as shown in Fig. 8. Fig. 11 shows the resonant frequency and the spring constant of the test structure with 40-μm-wide leaf-sprngs versus the temperature. The vertical axis is normalized at a value of 25 °C. It was found that the resonant frequency decreases monotonically with temperature at a rate of about 0.3%/°C, and is reduced by 21% at 80 °C. This corresponds to the reduction of the spring constant at 0.6%/°C. Therefore, temperature correction will probably be necessary for sensor applications. It is noted that this change in

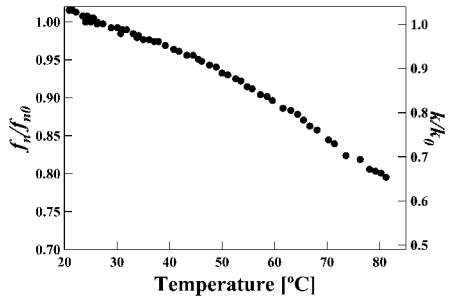

Fig. 11. The effect of temperature on the resonant frequency of the test structure using 40-μm-wide leaf springs. Vertical axis on the right represents the normalized spring constant.

the spring constant is reversible; a spring constant at the same temperature remains unchanged even after several thermal cycles between room temperature and 80 °C, which is slightly lower than the glass transition temperature of parylene-C of 80–100 °C.

IV. Prototype In-Plane Accelerometer

In order to demonstrate the advantages of the parylene high-aspect ratio beam, a prototype in-plane capacitive accelerometer was designed and fabricated. As shown in Fig. 12(a) and (b), a proof mass (9.4 mm × 6 mm) was supported by four leaf springs. The beam width and height were 20 and 400 μm, respectively. In order to measure the displacement of the proof mass with the capacitance change, grid electrodes were formed on the proof mass. Electrical contact between the proof mass and the external circuit was made through the parylene high-aspect- ratio beam. For this purpose, a second parylene deposition and etch-back were carried out in order to completely fill the void in the deep trench as shown in Fig. 2(c). After the second etch-back, a Cr/Au/Cr layer (100A/1000A/100A) is thermally deposited and patterned on the top of the 20-μm-wide beams. Another a parylene film of 2 μm in thickness was deposited on the top of the electrode as a protection layer. Width and spacing of the grid electrodes were 200 μm. The resistance between the substrate and the grid electrodes was 60 Ω. The resonant frequency measured was 37 Hz, which is in good agreement with the designed value of 35 Hz, as the trenches are fully filled with parylene.

The device chip with the proof mass was assembled with a glass chip with interdigitized counter electrodes as shown in Fig. 12(c). Fig. 12(d) shows the early prototype accelerometer, in which a differential-type readout IC (MicroSensors Inc., MS3110) with a low noise floor of 4 $\mathrm{aF}/(\mathrm{Hz})^{0.5}$ was used. Fig. 13 shows the circuit diagram of the present system.

Since it was difficult to precisely control the gap between the electrodes on the proof mass and the counter electrodes, the gap is as large as 100 μm. In this configuration, the mechanical sensitivity, which is the theoretical capacitance change to the in-plane acceleration, is 4.5 pF/g. Thus, the present prototype has almost the same sensitivity as the low-noise in-plane Si accelerometer developed by Chae *et al.* [20]

Fig. 14 shows the static response of the accelerometer to gravity by changing the tilt angle with respect to the gravitational direction. The overall sensitivity of this prototype was

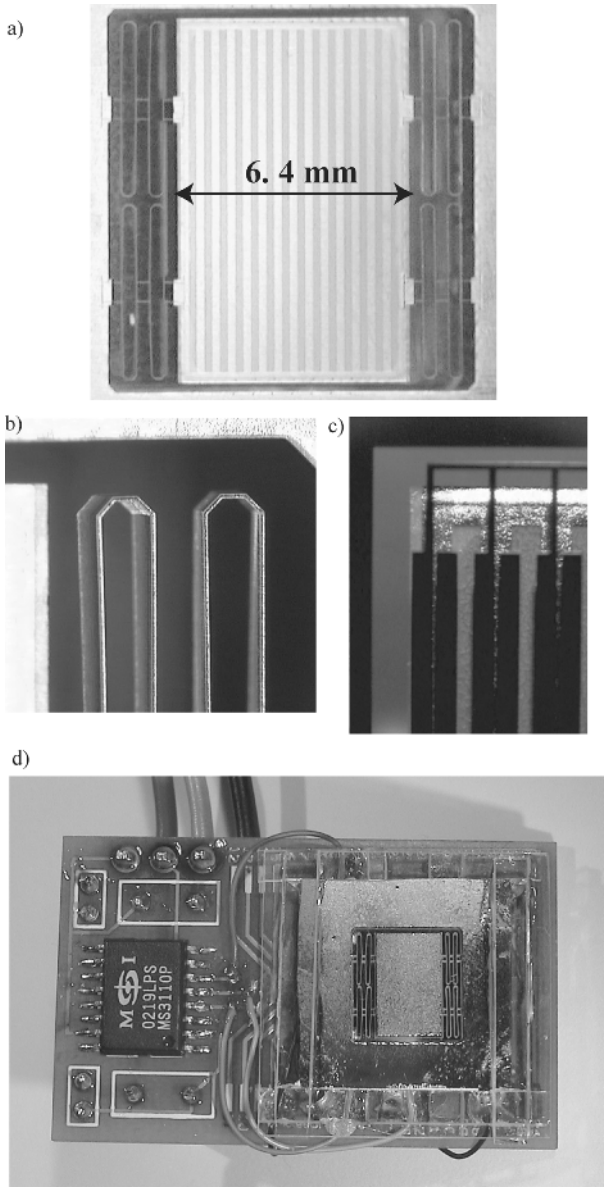

Fig. 12. Prototype of an in-plane capacitive accelerometer using high-aspect-ratio parylene springs. (a) Proof mass with grid electrodes and leaf springs. (b) Magnified view of the leaf spring (20-μm wide, 400-μm high). (c) Magnified view through the counter electrode. (d) Prototype device with a readout IC.

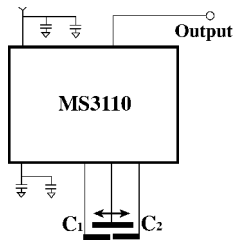

Fig. 13. Circuit diagram.

found to be $-1.333\ \mathrm{V/g}$, which is seven times smaller than the designed value. This is because the electrical sensitivity is poor; in the present design, the electrode width is only twice as large as the gap, so that a large fringe field should exist. Moreover,

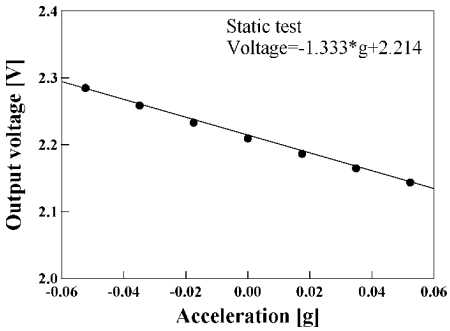

Fig. 14. Static response of the prototype accelerometer.

there is no guard electrode on the proof mass, which results in large parasitic capacitance.

It was also found that the noise floor of the present device was about 85 $\mu\mathrm{V}/(\mathrm{Hz})^{0.5}$, which results in the noise spectral density of 64 $\mu\mathrm{g}/(\mathrm{Hz})^{0.5}$, i.e., 6.3×10^{-4} $\mathrm{m/s^2(Hz)^{0.5}}$. Therefore, whereas the present accelerometer is still an early prototype, it already has a low-noise floor, aided by the low spring constant of the parylene beam. Note that the noise floor is about ten times larger than that of the readout IC at 8.4 $\mu\mathrm{V}/(\mathrm{Hz})^{0.5}$.

The Brownian equivalent acceleration noise $g_{n,B}$ is given by

$$g_{n,B} = \frac{\left(\frac{8\pi kT f_{\mathrm{res}}}{MQ}\right)^{0.5}}{g}, \quad \left[\frac{\mathrm{g}}{(\mathrm{Hz})^{0.5}}\right] \tag{1}$$

where k, T, and M are, respectively, the Boltzman constant, temperature, and the weight of the proof mass [30]. In the present accelerometer, $f_{\mathrm{res}} = 37$ Hz, which is the lowest resonant frequency among MEMS accelerometers ever built. Futhermore, the mass $M = 66$ mg is much larger than that of previous MEMS accelerometers. As a result, $g_{n,B}$ as given by (1) is as low as 25 $\mathrm{ng}/(\mathrm{Hz})^{0.5}$ or 2.5×10^{-7} $\mathrm{m/s^2(Hz)^{0.5}}$, which is three orders of magnitude smaller than the noise floor measured.

Since the noise level of the present accelerometer is not limited by Brownian noise, there exists considerable room to improve its sensitivity, especially the electrical sensitivity. For instance, when the gap between electrodes is reduced to 20 μm to suppress the fringe field, and the guard electrodes are formed on the proof mass to minimize the parasitic capacitance, the electrical sensitivity will jump to 48 V/g, which reduces the noise floor down to 1.8 $\mu\mathrm{g}/(\mathrm{Hz})^{0.5}$.

The dynamic response of the prototype was examined in a preliminary experiment. The prototype was fixed onto the moving stage of a shaker (Labworks Inc., LW-140-110), and shaken in the in-plane direction. The oscillation of the stage was measured with a laser displacement meter (Keyence Corp., LC-2440), and the output voltage of the readout IC is digitized with a 14-bit AD converter. Fig. 15 shows power spectra of the output voltage for a sinusoidal oscillation at 3 Hz. A sharp peak at the oscillation frequency can be observed. Since the present accelerometer is an underdamped system, a large peak is also observed at the resonant frequency.

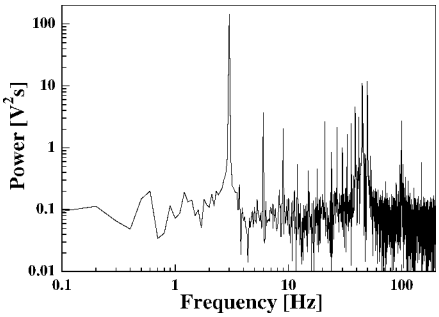

Fig. 15. Power spectra of output voltage for sinusoidal oscillation at 3 Hz.

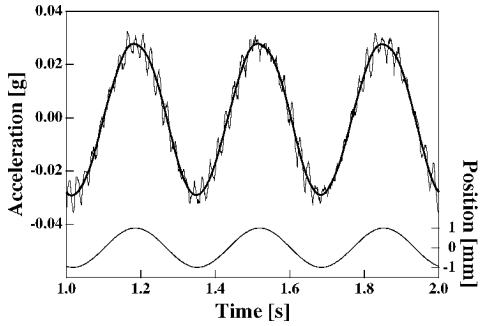

Fig. 16. Time trace of measured acceleration with sinusoidal oscillation at 3 Hz. The thick line represents filtered acceleration with a numerical low-pass filter at 20 Hz.

Fig. 16 shows a time trace of the acceleration measured. Sinusoidal oscillations at 3 Hz, having peak-to-peak amplitude of approximately 2 mm, are imposed, and the voltage output is converted into the acceleration using the static response shown in Fig. 14. An acceleration of around 50 $\mathrm{mg_{p\text{-}p}}$ at 3 Hz was successfully measured with the present prototype. Since the raw voltage signal includes fluctuations at the resonant frequency, a low-pass filter in Fourier space with a cut-off frequency of 20 Hz is used to remove the resonant frequency oscillation. The filtered data are also shown in Fig. 16, which are in good agreement with the imposed acceleration.

V. Conclusion

A new microfabrication technology for high-aspect-ratio parylene structure has been developed for soft spring applications, and its mechanical response has been fully characterized in a series of experiments. An early prototype in-plane accelerometer has been developed using parylene high-aspect-ratio springs. The following conclusions can be derived.

1) Free-standing parylene beams 10–40 μm in width with an aspect ratio of 10–20 can be fabricated.
2) A high-aspect-ratio beam with a spring constant of 0.0045 N/m has been developed.
3) In-plane oscillations with an amplitude as large as 600 $\mu\mathrm{m_{p\text{-}p}}$ has been achieved without any failure of the high-aspect ratio springs.
4) An early prototype of an in-plane capacitive accelerometer with a record-low resonant frequency of 37 Hz has been developed. It has also been demonstrated that the prototype accelerometer can measure acceleration of 50 mg peak-to-

peak amplitude at 3 Hz with a noise spectral density of 64 $\mu g/(\mathrm{Hz})^{0.5}$.

REFERENCES

[1] J. W. Weigold, K. Najafi, and S. W. Pang, "Design and fabrication of submicrometer, single crystal Si accelerometer," *J. Microelectromech. Syst.*, vol. 10, pp. 518–524, 2001.

[2] G. Genolet, M. Despont, P. Vettiger, D. Anselmetti, and N. F. de Rooij, "All-photoplastic, soft cantilever cassette probe for scanning force microscopy," *J. Vac. Sci. Technol., B*, vol. 18, pp. 617–620, 2000.

[3] N. Chronis and L. P. Lee, "Polymer MEMS-based microgripper for single cell manipulation," in *Proc. 17th IEEE Int. Conf. MEMS*, Maastricht, 2004, pp. 17–20.

[4] J. Lee, H. Shin, S. Kim, S. Hong, J. Chung, H. Park, and J. Moon, "Fabrication of atomic force microscope probe with low spring constant using SU-8 photoresist," *Jpn. J. Appl Phys.*, vol. 42, pp. L1171–1174, 2003.

[5] X. Xing, J. M. Yang, Y.-C. Tai, and C.-M. Ho, "Micromachined membrane particle filters," *Sens. Actuators, A*, vol. 73, pp. 184–191, 1999.

[6] L. Kicklider, X.-Q. Wang, A. Desai, Y.-C. Tai, and T. D. Lee, "A micromachined chip-based electrospray source for mass spectrometry," *Anal. Chem.*, vol. 72, pp. 367–375, 2000.

[7] T. N. Pornsin-sirirak, Y.-C. Tai, H. Nassef, and C.-M. Ho, "Titanium-alloy MEMS wing technology for a micro aerial vehicle application," *Sens. Actuators, A*, vol. 89, pp. 95–103, 2001.

[8] H. S. Noh, P. J. Hesketh, and G. C. Frye-Mason, "Parylene gas chromatographic column for rapid thermal cycling," *J. Microelectromech. Syst.*, vol. 11, pp. 718–725, 2002.

[9] T.-J. Yao, X. Yang, and Y.-C. Tai, "BrF3 dry release technology for large freestanding parylene microstructures and electrostatic actuators," *Sens. Actuators, A*, vol. 97, pp. 771–775, 2002.

[10] M. N. Niu and E.-S. Kim, "Piezoelectric bimorph microphone built on micromachined parylene diaphragm," *J. Microelectromech. Syst.*, vol. 12, pp. 892–898, 2003.

[11] J. Xie, J. Shih, Q. A. Lin, B. Z. Yang, and Y.-C. Tai, "Surface micromachined electrostatically actuated micro peristaltic pump," *Lab on Chip*, vol. 4, pp. 495–501, 2004.

[12] Z. Fan, J. M. Engel, J. Chen, and C. Liu, "Parylene surface-micromachined membranes for sensor applications," *J. Microelectromech. Syst.*, vol. 13, pp. 484–490, 2004.

[13] S. Dabral, J. Vanetten, X. Zhang, C. Apblett, G. R. Yang, P. Ficalora, and J. F. McDonald, "Stress in thermally annealed parylene films," *J. Electronic Mater.*, vol. 21, pp. 989–994, 1992.

[14] T. A. Harder, T.-J. Yao, Q. He, C.-Y. Shih, and Y.-C. Tai, "Residual stress in thin-film parylene-C," in *Proc. 15th IEEE Int. Conf. MEMS*, Las Vegas, 2002, pp. 17–20.

[15] G. Schropfer, S. Ballandras, M. deLabachelerie, P. Blind, and Y. Ansel, "Fabrication of a new highly-symmetrical, in-plane accelerometer structure by anisotropic etching of (100) silicon," *J. Micromech. Microeng.*, vol. 7, pp. 71–78, 1997.

[16] A. Partridge, J. K. Reynolds, B. W. Chui, E. M. Chow, A. M. Fitzgerald, L. Zhang, S. R. Cooper, T. W. Kenny, and N. I. Maluf, "A high performance planar piezoresistive accelerometer," in *Proc. Solid-State Sens. Actuator Workshop*, Hilton Head, SC, 1998, pp. 59–64.

[17] M. A. Lemkin, T. N. Juneau, W. A. Clark, T. A. Roessig, and T. J. Brosnihan, "A low-noise digital accelerometer using integrated SOI-MEMS technology," in *Proc. 10th Int. Conf. Solid-State Sens. Actuators (TRANSDUCERS '99)*, Sendai, Japan, 1999, pp. 1294–1297.

[18] H. Luo, G. Zhang, L. R. Carley, and G. K. Fedder, "A post-CMOS micromachined lateral accelerometer," *J. Microelectromech. Syst.*, vol. 11, pp. 188–195, 2002.

[19] X. Jiang, F. Wang, M. Kraft, and B. Boser, "An integrated surface micromachined capacitive lateral accelerometer with 2 $\mu g/\mathrm{rtHz}$ resolution," in *Proc. Solid-State Sens. Actuators Workshop*, Hilton Head, SC, 2002, pp. 202–205.

[20] J. Chae, H. Kulah, and K. Najafi, "An in-plane high-sensitivity, low-noise micro-g silicon accelerometer with CMOS readout circuitry," *J. Microelectromech. Syst.*, vol. 13, pp. 628–635, 2004.

[21] P. D. Mitcheson, T. C. Green, E. M. Yeatman, and A. S. Holmes, "Architectures for vibration-driven micropower generators," *J. Microelectromech. Syst.*, vol. 13, pp. 429–440, 2004.

[22] T. Tsutsumino, Y. Suzuki, N. Kasagi, and Y. Sakane, "Seismic power generator using high- performance polymer electret," in *IEEE Int. Conf. MEMS 2006*, Istanbul, Turkey, 2006, pp. 98–101.

[23] A. A. Ayon, R. Braff, C. C. Lin, H. H. Sawin, and M. A. Schmidt, "Characterization of a time multiplexed inductively coupled plasma etcher," *J. Electrochem. Soc.*, vol. 146, pp. 339–349, 1999.

[24] C. Keller and M. Ferrari, "Milli-scale polysilicon structures," in *Proc. Solid-State Sens. Actuator Workshop*, Hiton Head, 1994, pp. 132–137.

[25] D. A. Horsley, M. B. Cohn, A. Singh, R. Horowitz, and A. P. Pisano, "Design and fabrication of an angular microactuator for magnetic disk drives," *J. Microelectromech. Syst.*, vol. 7, pp. 141–148, 1998.

[26] F. Ayazi and K. Najafi, "High aspect-ratio combined poly and single-crystal silicon (HARPSS) MEMS technology," *J. Microelectromech. Syst.*, vol. 9, pp. 288–294, 2000.

[27] H. Guckel, "High-aspect-ratio micromachining via deep X-ray lithography," *Proc. IEEE*, vol. 86, pp. 1586–1593, 1998.

[28] J. B. Fortin and T.-M. Lu, "A model for the chemical vapor deposition of poly(para-xylylene) (Parylene) thin films," *Chem. Mater.*, vol. 14, pp. 1945–1949, 2002.

[29] B. Ilic, D. Czaplewski, M. Zalalutdinov, B. Schmidt, and H. G. Craighead, "Fabrication of flexible polymer tubes for micro and nanofluidic applications," *J. Vac. Sci. Technol., B*, vol. 20, pp. 2459–2465, 2002.

[30] J. Bernstein, R. Miller, W. Kelley, and P. Ward, "Low-noise MEMS vibration sensor for geophysical applications," in *Proc. Solid-State Sens. Actuator Workshop*, Hilton Head, SC, 1998, pp. 55–58.

Yuji Suzuki (M'01) received the B.S., M.S., and Dr. Eng. degrees in mechanical engineering from the University of Tokyo, Tokyo, Japan, in 1987, 1989, and 1993, respectively.

After spending one year at the Nagoya Institute of Technology as a Assistant Professor, he joined the Graduate School of Engineering, University of Tokyo. He is currently an Associate Professor with the Department of Mechanical Engineering, University of Tokyo. His research interests include power MEMS such as MEMS energy harvesting devices, active flow control with MEMS sensors and actuators, and microthermofluids systems such as microcatalytic combustor and MEMS cell sorting systems.

Dr. Suzuki is a Member of the American Society of Mechanical Engineers (ASME).

Yu-Chong Tai (M'97–SM'03–F'06) received the B.S. degree from National Taiwan University, Taiwan, and the M.S. and Ph.D. degrees in electrical engineering from the University of California at Berkeley in 1986 and 1989, respectively.

He then joined the faculty of Electrical Engineering, California Institute of Technology (Caltech), Pasadena, and built the Caltech Micromachining Laboratory. He is currently a full Professor of Electrical Engineering at Caltech. His research interests include flexible MEMS, integrated microfluidics, neuroprobes and chips, optical MEMS and biochemical sensors.